Desalination and Water Treatment
www.deswater.com
doi: 10.5004/dwt.2019.24345

162 (2019) 341–352
September

Evaluation of the removal of phenol from contaminated water by graphene oxide functionalized with polydiallydimethylammonium chloride (GPDADMAC)

Abideen O. Salawudeen[a], Bassam S. Tawabini[a,*], Tawfik A. Saleh[b], Abdulaziz M. Al-Shaibani[a]

[a]*Geosciences Department, College of Petroleum & Geosciences, King Fahd University of Petroleum & Minerals (KFUPM), Dhahran 31261, Saudi Arabia, Tel. +966 502145429; email: bassamst@kfupm.edu.sa (B.S. Tawabini), Tel. +966 506436680; email: g201513410@kfupm.edu.sa (A.O. Salawudeen), Tel. +966 546485825; email: shaibani@kfupm.edu.sa (A.M. Al-Shaibani)*
[b]*Chemistry Department, KFUPM, Dhahran 31261, Saudi Arabia, Tel. +966 506065323; email: tawfik@kfupm.edu.sa*

Received 8 November 2018; Accepted 26 April 2019

ABSTRACT

In this study, the removal of phenol from aqueous solution using synthesized graphene oxide functionalized with polydiallydimethylammonium chloride (GPDADMAC) adsorbent was investigated. Prior to adsorption experiments, the structural and chemical characteristics of the adsorbent were carried out using Fourier transform infrared spectroscopy, Brunauer–Emmett–Teller, scanning electron microscopy and energy dispersive X-ray spectroscopy techniques. About 80% removal of phenol was achieved within 10 min under the optimum conditions of 4 g L^{-1} adsorbent dosage, 10 mg L^{-1} initial phenol concentration, 298 K temperature, pH of 5.6 and agitation speed of 150 rpm. Results of the study also revealed that removal of phenol by GPDADMAC was almost independent of pH within the range of 4–9. The experimental data were best described by the pseudo-second-order kinetic model which implied that the rate-limiting step was the chemisorption. Based on isotherm modeling, both Langmuir and Temkin isotherm models produced the best fit for the experimental data. The thermodynamic parameters showed that the adsorption process was exothermic.

Keywords: Adsorption; Functionalization; Nanomaterial; Graphene oxide; Phenol; Polydiallydimethylammonium chloride

1. Introduction

Phenol is one of the priority pollutants that calls for great attention due to its toxic nature, persistence in the environment, biomagnification in organisms and damaging health effects in human [1,2]. The ingestion of water contaminated with phenol over a long period of time causes destruction of body protein and tissues, dysfunction of the central nervous system and damages to the gastrointestinal tract.

As water regulations and standards become more stringent, it is paramount that phenol is removed from contaminated water. Common technologies used to remove phenol include photocatalytic degradation [3], ozonation [4], extraction method [5], biological method [6], membrane-based separation [7], electrochemical advanced oxidation method [8] and ion exchange [9]. These methods have their drawbacks which include huge costs, partial degradation, and generation of secondary pollutants and toxic sludge. Consequently, adsorption is considered as one of the appropriate techniques for the removal of phenol from water due to its inexpensiveness and effectiveness. Also, the technique produces no toxic wastes. However, its performance is highly constrained by material design and properties [10].

* Corresponding author.

Carbon-based materials such as activated carbon (AC) have been always used as adsorbents [11,12]. However, their activity is limited to the size of the surface area. Recently, there is a rise in the application of nanobased materials for the removal of toxic pollutants [13–16]. Among the nanomaterials, the use of graphene for wastewater remediation is gaining more popularity [17–21]. Graphene is an allotrope of carbon consisting of a single layer of carbon atoms arranged in a hexagonal lattice. It is considered an excellent adsorbent due to its unique characteristics such as high specific surface area and ease of synthesis from graphite using an uncomplicated and cheap method involving chemical oxidation, exfoliation and reduction. It has been applied for the adsorption of several pollutants, such as dyes [22], metal ions [23] and organic pollutants [24].

The tendency of graphene and its derivatives to aggregate to reform graphite and their weak affinity for binding anionic pollutants are considered disadvantages to their applications. Nevertheless, these disadvantages can be surpassed by covalent or non-covalent functionalization with different molecules. This surface functionalization makes graphene and its derivatives more sensitive, selective and detective. Due to the availability of many materials that can be used for surface functionalization, there are always growing opportunities to study potential applications of these materials in the adsorptive treatment of wastewater [25]. So far, a number of functionalized graphene, graphene oxide (GO) and reduced graphene oxide (RGO) have been successfully synthesized and extensively investigated as adsorbents for water purification [18,19].

Materials used for functionalization of graphene include organic polymers and nanosized metal oxide [26,27]. These materials can be grafted on the surface without any requirement of crosslinkers which usually reduce the binding sites for pollutants. The extensive literature search did not reveal any study where GO is functionalized with PDADMAC for phenol removal.

Therefore, this study investigates the removal efficiency of GO functionalized with polydiallydimethyl ammonium chloride (GPDADMAC) for phenol removal from water. The effects of various parameters such as temperature, pH, contact time, adsorbent dosage, initial concentration of phenol and agitation speed were optimized. The obtained data were modeled using Freundlich, Langmuir and Temkin isotherm models. Also, the kinetics were studied, and the thermodynamic parameters were obtained.

2. Experimental

2.1. Synthesis of graphene oxide

Graphene oxide was prepared from graphite powder according to the Hummer's method. 1.8 g of potassium persulfate ($K_2S_2O_8$) and 3 g of natural graphite powder were added into 100 mL sulfuric acid (H_2SO_4) in an ice–water bath, under stirring. Then, the mixture was heated to around 90°C in an oil bath after which the system was allowed to cool. After that, 9 g of $KMnO_4$ were added into the flask slowly. The system was heated at around 40°C under stirring. Water and hydrogen peroxide (30%) were carefully added till the brownish color was observed. The mixture was then filtered and washed with diluted 2 M HCl aqueous solution to remove metal ions. The synthesized graphene oxide was collected and dried in vacuum freezing drying oven for 2 d.

2.2. Synthesis of polydiallydimethylammonium chloride (PDADMAC)-graphene oxide

First, the monomer was created by reacting equivalent amounts of allyl chloride and dimethylamine. The polymer was produced by radical polymerization of diallyldimethylammonium chloride in presence of graphene of which the functional groups were utilized to host the monomer. Then, organic peroxide was introduced to the system as a catalyst for radical polymerization. When polymerizing diallyldimethylammonium chloride, one side of the polymer chain is chemically bonded on graphene and the chain is grafted, as shown in Fig. 1.

2.3. Instruments for characterization

FESEM/energy dispersive X-ray spectroscopy (EDX) (TESCAN LYRA3) was used for the characterization of the surface morphology of both GO and GPDADMAC. The determination of the surface area and porous distribution was carried out by nitrogen physisorption at 77°C using Micromeritics ASAP 2000 system (USA). Functional groups detection for both GO and GPDADMAC was done using Fourier transform infrared spectroscopy (FTIR) spectrum produced by FTIR Spectrometer (Nicolet 5700) over the wavenumber range from 4,000 to 400 cm^{-1}. The samples for FTIR were pelletized using pressed disks to grind and mix GO or GPDADMAC with KBr in an agar mortar.

2.4. Reagents and analytical measurement

All reagents used were of analytical grade. A stock solution of adsorbate was prepared by dissolving 1 g of phenol (Sigma-Aldrich, USA, >99%) in 1,000 mL of ultrapure deionized water (Milli-Q Ultrapure water system, Millipore). Thereafter, working solutions of desired concentrations ranging from 5 to 50 mg L^{-1} were prepared in clean conical flasks by diluting an appropriate volume of

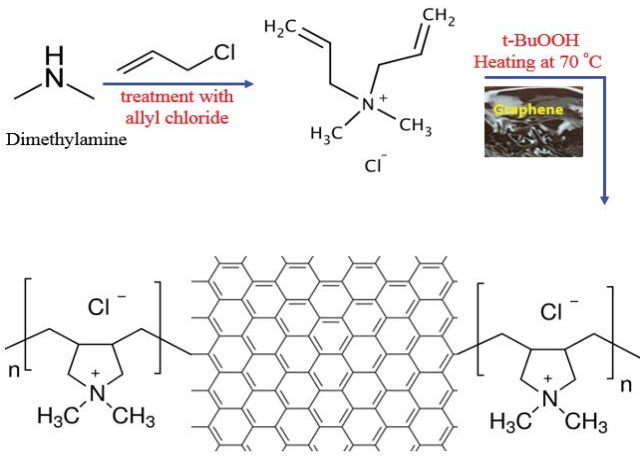

Fig. 1. Illustration of the process of the synthesis of polydiallydimethylammonium chloride modified graphene (PDADMAC).

the stock solution with an appropriate volume of DI water. Before every experimental run, the initial concentrations were measured using UV spectrophotometer (SPECORD-50, Analytik Jena, Germany) at a wavelength of 271 nm following the method used by Roig et al. [28]. The calibration of the UV spectrophotometer was done using prepared standards of phenol concentration range between 0 and 100 mg L^{-1}. A linear calibration curve of absorbance against phenol concentration with R^2 equal 0.999 was obtained. For experiments requiring pH adjustment, 0.1 M HCl (Merck, Suprapure, Germany) or 0.1 M NaOH (Merck, Suprapure, Germany) solution was used and the pH was ascertained by benchtop pH meter (A0057419, Hanna Instruments, USA).

2.5. Determination of point of zero charge

The point of zero charge (PZC) for GPDADMAC was determined by following the procedure by Thirumavalavan et al. [29]. An Erlenmeyer flask was filled with 100 mL of deionized (DI) water and capped with cotton wool. This was heated until boiling for about 30 min to expel all carbon dioxide and dissolved ions in the water. Immediately after cooling, the flask was capped with a rubber stopper to prevent carbon dioxide from entering. 10 mL of this carbon dioxide free DI water was added to about 30 mg of the adsorbent, sealed and shaken for 48 h at room temperature of 25°C. The final pH of the solution was measured and taken as the PZC of the adsorbent.

2.6. Treatment studies

Batch experiments were conducted in order to investigate the removal efficiency of GPDADMAC for phenol. For each experiment, 50 mL of an aqueous solution of phenol in 250 mL Erlenmeyer flasks was used to study the effect of contact time, initial solution pH, initial concentration of phenol, adsorbent dosage, agitation speed and temperature. A 0.45 μm filter was used to obtain a filtrate after every experimental run. UV spectrophotometer at 271 nm wavelength was used to analyze the concentration of phenol. To ensure repeatability, the mean of duplicates was used in the computation of percentage removal as well as adsorption capacity as per the following equations [30]:

$$\%\ \text{phenol removal} = \frac{\left(C_i - C_f\right)}{C_i} \times 100 \tag{1}$$

$$\text{Adsorption capacity} = \left(C_i - C_f\right) \times \frac{V}{m} \tag{2}$$

C_i and C_f (mg L^{-1}) stand for initial and final concentrations whereas V (mL) and m (mg) are the volumes of aqueous solution containing phenol and mass of adsorbent respectively.

2.7. Adsorption isotherms

In order to design a suitable industrial adsorption system, it is crucial to know the distribution of adsorbate molecules between the adsorbent and the adsorbate solution as well as the interactions between both [31]. Towards this end, several adsorption isotherm models are applied on adsorption data to obtain the best-fit models. Application of isotherm models is based on the general assumptions concerning the type of interaction between the adsorbate and the adsorbent, number, and nature of adsorbent layers involved in adsorbing the adsorbate. Langmuir, Freundlich, and Temkin are some of the empirical isotherm models mostly applied to single solute systems carried out in batch mode. Langmuir isotherm model [32] is linearly expressed as:

$$\frac{C_e}{q_e} = \frac{1}{K_L \times q_m} + \frac{q_e}{q_m} \tag{3}$$

where K_L (L mg^{-1}) is the constant for sites of adsorption affinity on homogenous monolayer surface, q_m (mg g^{-1}) is the maximum monolayer adsorption capacity, q_e (mg g^{-1}) is the amount of adsorbate adsorbed, C_e (mg L^{-1}) is the equilibrium concentration of adsorbate in solution. The values of q_m and K_L are obtained from the slope and intercept of a plot of C_e/q_e against C_e. Separation factor in Langmuir model is an important parameter given as:

$$R_L = \frac{1}{\left(1 + K_L \times C_0\right)} \tag{4}$$

where C_0 (mg L^{-1}) is the initial concentration of the adsorbate. The value of R_L is interpreted as follows: Value of 1 is an indication of linear adsorption, a value greater than 1 indicates an unfavorable adsorption process, between 0 and 1 means favorable adsorption process while equal to 0 indicates irreversible adsorption process [31]. The linear mathematical form of Freundlich isotherm model is as follows:

$$\ln q_e = \ln K_F + \frac{1}{n} \ln C_e \tag{5}$$

where K_F (mg g^{-1}) represents Freundlich isotherm constant that indicates adsorption capacity. The heterogeneity parameter, n, gives the description of adsorption intensity. A value of n equal to 1 indicates linear adsorption where all adsorption sites have the same sorption energies. When n is greater than 1, it implies a normal and favorable adsorption process and the higher its value, the stronger is the adsorption. C_e (mg L^{-1}) and q_e (mg g^{-1}) are the adsorbate concentration in solution and amount of adsorbed adsorbate on the adsorbent, respectively. Temkin isotherm model in its linear mathematical expression is as follows:

$$q_e = \frac{RT}{b_T} \ln K_T + \frac{RT}{b_T} \ln C_e \tag{6}$$

b_T (J mol^{-1}) represents Temkin isotherm constant for sorption heat, K_T (L g^{-1}) is the binding constant describing the highest binding energy while T (K) and R are temperature and gas constant, respectively.

2.8. Kinetic study

For an adsorption process, different mechanisms and factors control the rate of sorption of adsorbate on the

adsorbent and these include mass transfer and chemical process [32]. Therefore, to examine and validate the most probable mechanisms and potential rate-controlling stages, adsorption experimental data are tested by different kinetic models. The linearized mathematical expression for the pseudo-first-order is represented as:

$$\log\left(q_e - q_t\right) = \log\left(q_e\right) - \frac{k_1}{2.303}t \tag{7}$$

q_e and q_t denote, respectively, the amounts of phenol adsorbed in mg g^{-1} at equilibrium and at time t (min). The value of the rate constant k_1 is calculated from the slope while that of parameter q_e is derived from the intercept of the same graph of log ($q_e - q_t$) against t. Pseudo-second-order linear equation is applied as follows:

$$\frac{t}{q} = \frac{t}{q_e} + \frac{1}{k_2}q_e^2 \tag{8}$$

where q and q_e denote the amounts of phenol adsorbed (mg g^{-1}) by GPDADMAC at time t (min) and at equilibrium. Values of equilibrium rate constant k_2 and parameter q_e are derived from the slope and intercept of a plot of t/q against t. Intraparticle diffusion model based on the following equation is used:

$$q_t = C_i + k_{id} \times t^{1/2} \tag{9}$$

where k_{id} and C_i are the rate constant and model constant obtained from the slope and intercept of the plot of q_t against $t^{1/2}$ at stage i.

2.9. Thermodynamics

Thermodynamic models provide useful information on the inherent energetic changes during the adsorption process through the parameters of Gibbs free energy change (ΔG), isosteric enthalpy change (ΔH) and entropy change (ΔS). The isosteric enthalpy change can be obtained from the derivative of Van't Hoff's expression [33]:

$$\ln K_0 = \frac{\Delta S}{R} - \frac{\Delta H}{RT} \tag{10}$$

$$K_0 = \frac{q_e}{C_e} \tag{11}$$

where K_0 (g L^{-1}) is the distribution coefficient of adsorbate in solution, ΔH (J mol^{-1}) is the isosteric adsorption enthalpy change, T (K) is the absolute temperature, R is the ideal gas constant (8.314 J mol^{-1} K^{-1}). The Gibbs free energy change is calculated from the following equations:

$$\Delta G = -RT \ln K_0 \tag{12}$$

3. Results and discussion

3.1. Characterization

3.1.1. Surface morphological analysis of GPDADMAC

Textural properties of GPDADMAC were investigated by applying the N_2-physisorption analysis. The Brunauer–Emmett–Teller (BET) isotherm plot and the pore size distribution are presented in Figs. 2a and b, respectively. Following the IUPAC classification of adsorption isotherms [34], GPDADMAC isotherm plot is similar to the type II isotherm curve which is characterized by uniform surface energy and multilayer adsorption. As suggested by its adsorption of nitrogen at a low relative pressure range of 0–0.027, GPDADMAC has a microporous structure with monolayer physisorption. The change in adsorption from a monolayer to multilayer approximately occurs at the relative pressure range of 0.027–0.32. There is a slow increase in the quantity of nitrogen adsorbed at a pressure range of 0.32–0.82 which is an indication of the occurrence of multilayer adsorption. The sharp increase in nitrogen adsorption from relative pressure of 0.82 until saturation at 1 suggests the presence of macropores in GPDADMAC. The Type H3 hysteresis loop at a relatively high-pressure range indicates the mesoporous structure of GPDDA. Summing up, there is an indication

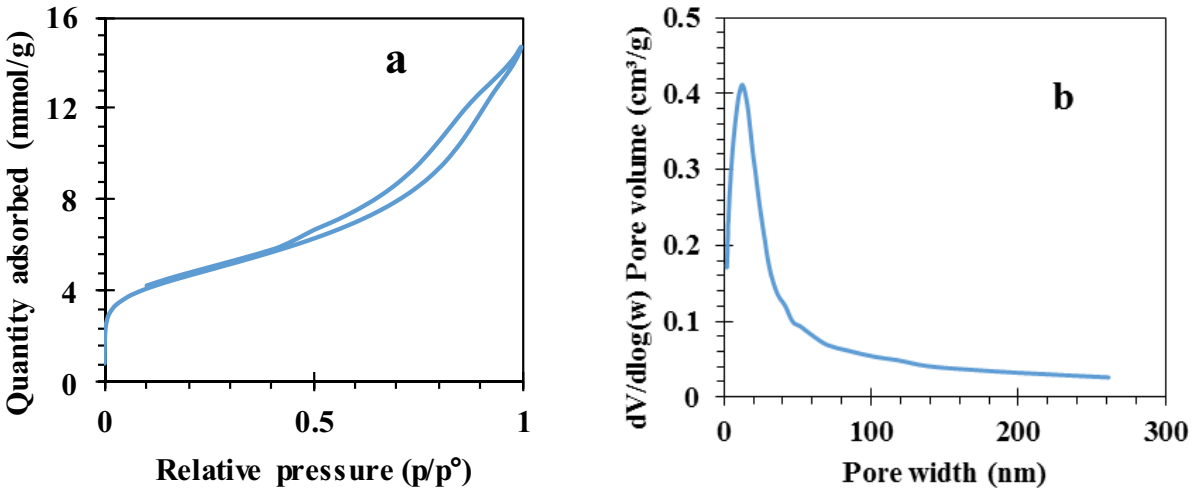

Fig. 2. (a) Nitrogen adsorption isotherms at 77 K and (b) Pore size distribution curve.

that the pore system of GPDADMAC is characterized by micropores, mesopores and macropores. Table 1 gives a summary of other parameters obtained from the analysis. The BET surface area of GPDADMAC was 357.4 $m^2 g^{-1}$ which is higher than that of GO and other similar nanoadsorbent such as CNT reported by Li et al. [35]. Meanwhile, the pore size distribution as shown in Fig. 2b indicates that GPDADMAC has a size that falls within the range of 2–50 nm, confirming the preponderance of mesopores in the material. This may allow the phenol to have more access to the inner layers of GPDADMAC for adsorption.

3.1.2. Scanning electron microscopy and EDX characterization

Fig. 3a is the scanning electron microscopy (SEM) image of GPDADMAC which reveals a porous network with a fluffy sponge-like structure that is different from the compact structure of exfoliated layer structure GO reported by Soleimani et al. [36]. This kind of structure increases the volume and also the area of GPDADMAC which may play a significant role in increasing the adsorption of phenol. More than 50% of the particle was of the size 3.2 nm which means that GPDADMAC is a nanomaterial.

Concerning the average elemental composition of GPDADMAC, the EDX spectrum in Fig. 3b shows that it comprises carbon (63.97%), oxygen (20.29%) and nitrogen (15.74%) within the spots inspected. In contrast to the EDX spectrum of graphene oxide reported by Şinoforoğlu et al. [37], the presence of nitrogen may be inferred to come from the PDADMAC molecule and this can indicate that the graphene oxides are successfully functionalized by PDADMAC.

Table 1
Parameters of nitrogen sorption analysis

Parameters	Values
BET surface area[a]	357.4 $m^2 g^{-1}$
External surface area[b]	290.5 $m^2 g^{-1}$
Micropore and mesopore volume[c]	0.46 $cm^3 g^{-1}$
Micropore volume[b]	0.036 $cm^3 g^{-1}$
Mesopore and macropore volume[d]	0.442 $cm^3 g^{-1}$
Mesopore volume	0.422 $cm^3 g^{-1}$
Macropore volume	0.020 $cm^3 g^{-1}$
Average pore diameter[a]	51.25 Å

[a]Obtained by BET.
[b]Obtained from the *t*-plot.
[c]Taken from the volume of nitrogen adsorbed at about $P/P_0 = 0.95$.
[d]By BJH.

3.1.3. FTIR characterization

Fig. 4 depicts the IR spectra of GO and GPDADMAC. It can be observed that GO contains oxygen functional groups on its surface as evidenced by the hydroxyl groups at ~3,441 cm^{-1}, a carboxyl group at ~1,730; ~1,381 and ~1,026 cm^{-1} as well as an epoxy group at ~838 and ~1,154 cm^{-1}. The IR spectrum of GPDADMAC showed some modifications in the form of shifts, decrease and complete disappearance as well as the appearance of new IR peaks when compared with that of GO.

There is a downward shift of the peaks attributed to hydroxyl group from ~3,441 in GO to ~3,416 cm^{-1} in GPDADMAC; carboxyl group from ~1,729 to ~1,716 cm^{-1}; aromatic ring from ~1,623 in GO to ~1,609 cm^{-1} in GPDADMAC; upward shift of carboxyl group from ~1,026 to ~1,028 cm^{-1} and unattributable peaks from ~759 to ~785. There is also an increase in the intensity of the peak attributed to alkyl group at ~2,920 cm^{-1} and disappearance of CN group peak at ~1,259 cm^{-1} and unattributable peak at ~1,454 cm^{-1}. This suggests that the interactions of GO and PDADMAC bring about reduction or modification of activities of vibrational modes in the mixture [38]. The disappearance of epoxy group peaks at ~838 and ~1,154 cm^{-1} and carboxyl group peaks at ~1,381 cm^{-1} in GPDADMAC indicates the reduction

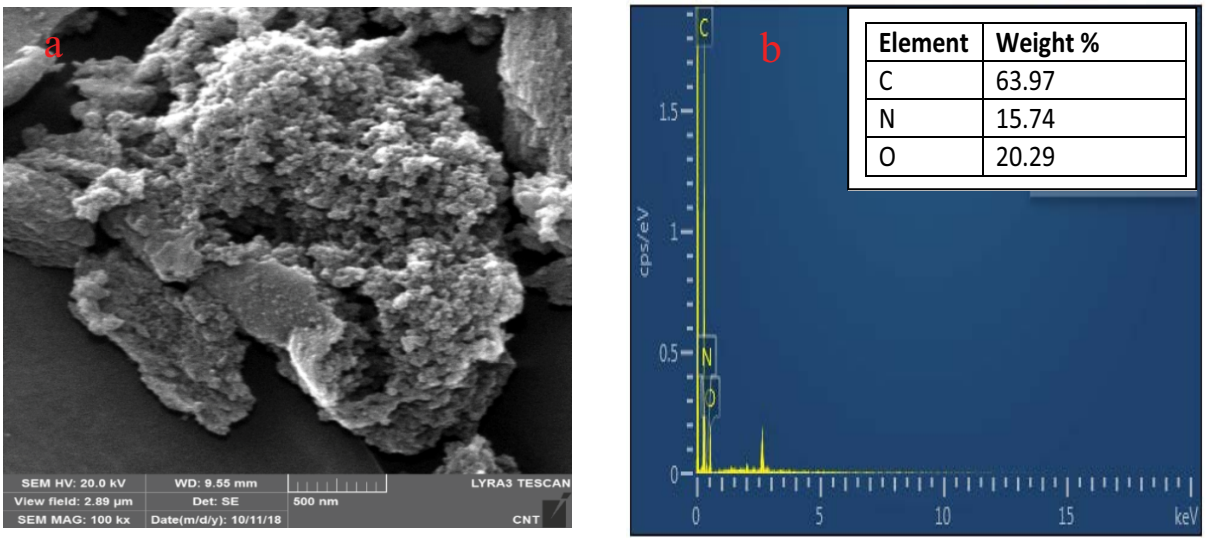

Fig. 3. (a) SEM image of GPDADMAC and (b) EDX spectrum of GPDADMAC.

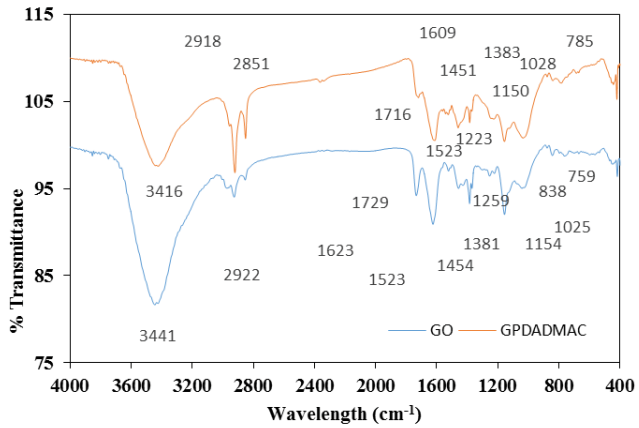

Fig. 4. FTIR spectra of GO and GPDADMAC.

in the number of oxygen functional groups of GO [39]. Meanwhile, the appearance of the characteristic peaks of PDADMAC in GPDADMAC, such as CH*n* group between ~2,918 and 2,850 cm^{-1}, C=C group at ~1,609 cm^{-1}, NO group at ~1,383 cm^{-1} and CN group at ~1,150 cm^{-1}, indicates that GO was successfully functionalized with PDADMAC [32]. The results are similar to those reported by Yang et al. [38], Țucureanu et al. [39], Ding et al. [40], Li et al. [41,42], Huang et al. [43], Coates [44].

3.1.4. Interaction mechanism between phenol and GPDADMAC

A comparison of the FTIR spectra of GPDADMAC before and after the adsorption (Fig. 5) revealed the possible interaction responsible for the adsorption of phenol by GPDADMAC. A slight upward shift in IR wavelength indicating hydroxyl group from 3,416 to 3,418 cm^{-1} was noticed after adsorption. This observation is similar to that reported by Yu et al. [45] and Ren et al. [46]. This may suggest the existence of hydrogen bonding between the hydroxyl group on phenol molecules and the oxygen-containing functional groups on GPDADMAC supplied by both GO and PDADMAC as well as the amino group provided by PDADMAC.

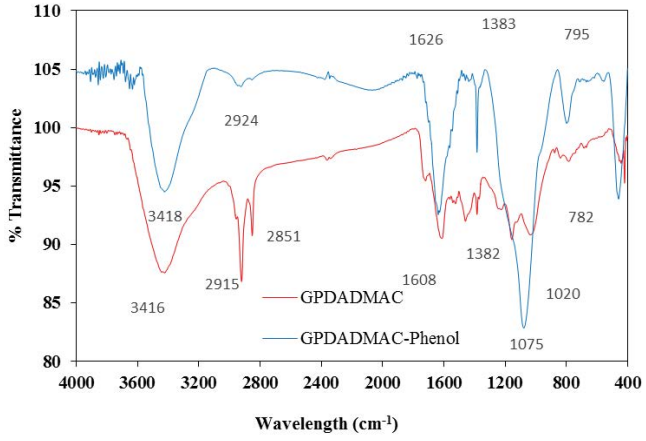

Fig. 5. FTIR spectra of GPDADMAC before and after adsorption.

Furthermore, there was a shift in the IR peak of the stretching vibration of C=C band from 1,609 to 1,626 cm^{-1} after adsorption as well as that of CH*n* from 2,915 to 2,924 cm^{-1} after adsorption. This is an indication of the presence of π–π interaction between GPDADMAC and phenol. As pointed out by McDermott and McCreery [47] that the surface central regions of graphene are typically deficient of electrons. Therefore, the phenyls of the phenol molecules which has abundant π-electrons can donate to the GPDADMAC that is deficient of π-electrons. The similar observation that π–π interaction enhance sorption of aromatic compounds containing hydroxyl groups were made by Wang et al. [48] and Chen et al. [49]

3.2. Adsorption experiment

3.2.1. Effect of contact time

Fig. 6a depicts the effect of contact time on adsorption of phenol by GPDADMAC, which was obtained under the varying time of 1–30 min at three different concentrations. Obviously, GPDADMAC is a very fast adsorbent for the removal of phenol from aqueous solution. The removal of phenol was very quick within the first 5 min with about 80% phenol adsorbed. However, its phenol removal efficiency became gradual beyond 5 min until equilibrium was reached at about 10 min.

The huge surface areas conferred on the GO by PDADMAC forming a fluffy sponge-like structure which allowed accumulation of many phenol molecules can be responsible for the exceptional initial fast adsorption rate observed. It is also possible that the availability of hydrophobic cavities formed from the opposite orientation between the cluster of ionic parts and the cluster of hydrophobic parts of the PDADMAC monomer units houses sparingly soluble phenol molecules. Meanwhile, as time passed, the space in the fluffy sponge-like structure and hydrophobic cavities got reduced as most of them were already being occupied by phenol molecules, thereby resulting in slow adsorption rate observed between 5 and 10 min. Eventually, when they were completely saturated with phenol molecules around 10 min, the equilibrium was reached with [26,50]. Therefore, the optimum contact time was chosen to be 10 min.

3.2.2. Effect of pH

Phenol removal by GPDADMAC was investigated within the pH range of 3–10. As shown in Fig. 6b, the removal percentage of phenol increased from 62% to 79% as the pH was raised from 3 to 4. However, there was a fairly constant removal percentage from pH of 4–9. Thereafter, a decrease in removal efficiency was noticed from pH 9–10. This trend is similar to that reported by Abdelwahab and Amin [51].

The PZC of GPDADMAC was measured to be 3.5. This means that the material surface was positively charged below 3.5 while it was negatively charged above 3.5. Hence, the lower removal efficiency recorded at pH 3 can be due to abundant positive charges on GPDADMAC surface resulting in static repulsion forces. On the other hand, it is most likely that there is no electrostatic interaction between the negative charge of GPDADMAC and the phenol at any pH value above 3.5 (PZC) and below 10 since phenol

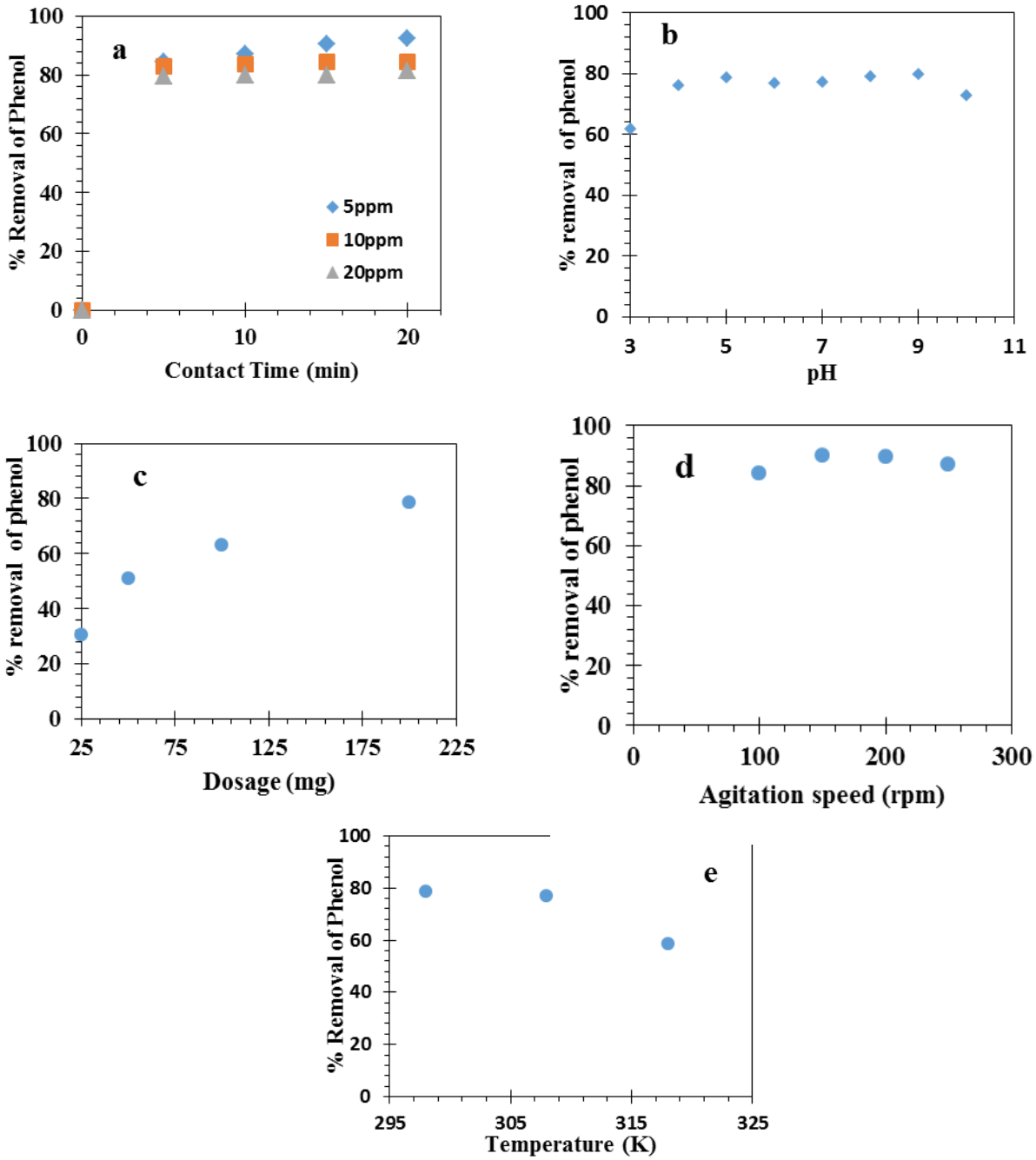

Fig. 6. Effect of (a) contact time on phenol removal at various initial concentration of phenol (adsorbent dosage = 200 mg, agitation speed = 150 rpm, temperature = 298 K and pH = 5.8), (b) pH on phenol removal (initial concentration of phenol of 10 ppm, adsorbent dosage = 200 mg, agitation speed = 150 rpm, temperature = 298 K and contact time = 30 min), (c) GPDADMAC dosage on phenol removal (initial conc of phenol = 10 ppm, contact time = 30 min, agitation speed = 150 rpm, Temperature = 298 K and pH = 5.8), (d) agitation speed on phenol removal (initial concentration of phenol = 10 ppm, adsorbent dosage = 200 mg, temperature = 298 K, contact time = 30 min and pH = 5.8), and (e) temperature on phenol removal (initial concentration of phenol = 10 ppm, adsorbent dosage = 200 mg, agitation = 150 rpm, contact time = 30 min and pH = 5.8).

exists as neutral molecules below its pKa of 10. Therefore, it is possible that the removal of neutral phenol molecules within pH of 4–9 is due to the existence of dispersive interactions between the aromatic ring of phenol and the basal planes of GPDADMAC replenished with a high π-electron density [52]. The fairly constant removal efficiency at the pH range of 4–9 can be an indication of the PDADMAC coating stabilizing and reducing the rolling-up of the graphene in aqueous solution [26,53]. Meanwhile, the fall in removal efficiency above pH 9 can be attributed to the repulsive

forces between phenolate anions and the negatively charged surface of GPDADMAC.

3.2.3. Effect of GPDADMAC dosage

As illustrated in Fig. 6c, the effect of adsorbent dosage from 25 to 200 mg was studied. There was an increase in phenol removal as the adsorbent dosage was increasing. A significant rise from 30% to 79% can be observed as the dosage was increased from 25 to 200 mg.

The observed increasing phenol removal by GPDADMAC as dosage increased can be associated with the availability of an increasing number of adsorption sites when the amount of adsorbents was increased [1,54]. However, it can also be noticed that the removal percentage was increasing at a decreasing rate because the number of phenol molecules remaining in the solution for adsorption by further increased dosage kept decreasing. In other words, the adsorption is tending towards equilibrium between adsorbed phenol molecules by GPDADMAC and unadsorbed phenol molecules in the solution as dosage increased [55].

3.2.4. Effect of agitation speed

The influence of agitation speed on the removal of phenol by GPDADMAC was investigated from 100 to 250 rpm. From Fig. 6d, the percentage phenol removal by GPDADMAC increased as the agitation speed was raised from 100 to 150 rpm which can be as a result of improved contact between phenol molecules and adsorption sites of GPDADMAC. However, the removal efficiency remained constant between 150 and 200 rpm which is an indication of saturation of the adsorption sites of GPDADMAC by phenol molecules. A further increase of agitation speed from 200 to 250 rpm resulted in a decrease in percentage removal of phenol. This observation can be as a result of desorption of already adsorbed phenol molecules from active sites caused by disturbance of equilibrium by further agitation.

3.2.5. Effect of temperature

The influence of changing temperature from 298 to 318 K on phenol adsorption by GPDADMAC was investigated. An increase in temperature from 298 K results in a decrease in the amount of phenol adsorbed by GPDADMAC (Fig. 6e). This can be attributed to an increase in average kinetic energy of phenol molecules as a result of temperature increase which leads to disturbance of the stability of the phenol-GPDADMAC complex and thereby causing desorption instead of adsorption [55]. It can also be inferred that phenol adsorption by GPDADMAC may be exothermic and that the best performance of GPDADMAC for phenol removal can be obtained at room temperature.

3.3. Kinetic study

Adsorption data are fitted into pseudo-first-order, pseudo-second-order and intraparticle diffusion kinetic models, Fig. 7. The calculated values of the rate constant k_1 and parameter q_e for the pseudo-first-order model are presented in Table 2. The relatively low value of R^2 (0.9221) can be an indication that the adsorption of phenol on GPDADMAC is not well represented by pseudo-first-order model.

Table 2
Parameters of kinetic models for the adsorption of phenol by GPDADMAC

Kinetic model	Parameters	Value
Pseudo-first-order	q_e (mg g^{-1})	0.610
	k_1 (min^{-1})	0.085
	R^2	0.922
	q_e experimental (mg g^{-1})	1.65
Pseudo-second-order	q_e (mg g^{-1})	3.224
	k_2 (g mg^{-1} min^{-1})	1.649
	R^2	0.999
	q_e experimental (mg g^{-1})	1.65
Intraparticle diffusion	k_1 (mg g^{-1} min$^{-1/2}$)	2.514
	R^2	1.0
	k_2 (mg g^{-1} min$^{-1/2}$)	0.35
	R^2	0.9823
	k_3 (mg g^{-1} min$^{-1/2}$)	–0.0246
	R^2	0.1422
	q_e experimental (mg g^{-1})	1.65

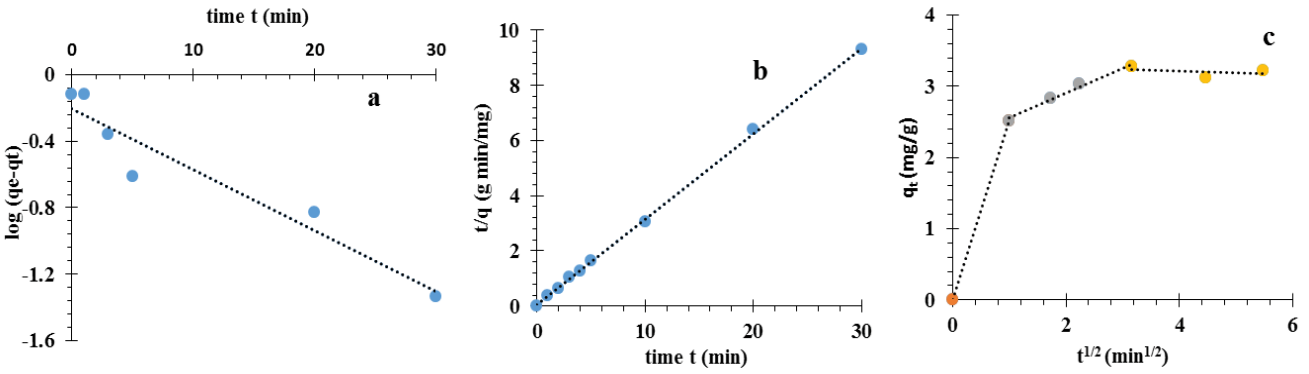

Fig. 7. (a) Pseudo-first-order model, (b) pseudo-second-order model, and (c) intraparticle diffusion model (adsorbent dosage = 4 g L^{-1}, initial phenol concentration = 20 mg L^{-1}, agitation speed = 150 rpm, temperature = 298 K, pH = 5.8).

Fig. 7b displays the fit of the adsorption data on pseudo-second-order model. Values of equilibrium rate constant k_2 and parameter q_e, are provided in Table 2. The resulting fitted straight line gives an indication that pseudo-second-order model well represents the adsorption process. Moreover, the high value of R^2 (0.9994) and the similarity between the calculated q_e and experimental q_e further support the validity of the model for the adsorption process of phenol on GPDADMAC. The adsorption of phenol on GPDADMAC is most likely monolayer with chemical processes controlling the adsorption rate.

As shown in Fig. 7c, the Weber's intraparticle diffusion model is characterized by multilinearity with three different stages. The first stage is the external surface adsorption wherein adsorbate ions are transported from the boundary film to the external surface of the adsorbate and this was completed within the first 4 min. The second stage wherein the adsorption process is being controlled by intraparticle diffusion was observed in less than 10 min. The intraparticle diffusion started declining in the third portion of the plot. The multilinearity of the model as well as the deviation of the trend lines of the three stages from the origin (Fig. 7c) due to the difference in mass transfer of the first and last stage suggest that the adsorption of phenol on GPDADMAC is not only controlled by intraparticle diffusion.

3.4. Isotherm models

Fig. 8 shows the plots of Langmuir, Freundlich and Temkin isotherm models, respectively, while Table 3 gives the summary of the parameters of the three models. As it can be observed in Table 3, the Langmuir and Temkin models show a good fit with correlation coefficients greater than 0.99, which means that the adsorption of phenol molecules by GPDADMAC can be explained by the two models. Based on the Langmuir model (Fig. 8a), it implies that there is a strong attachment of phenol molecules onto a limited number of adsorption sites with homogenous sorption energies present on a single surface layer of GPDADMAC. The maximum adsorption capacity as calculated from Langmuir was 4.54 mg g^{-1}. Furthermore, the value of separation factor, R_L, which is between 0 and 1, indicates that the adsorption of phenol on the GPDADMAC is favorable.

Comparing with Freundlich model, Fig. 8b, the good fit shown by the adsorption experimental data on Temkin model (Fig. 8c) indicates that an increase in the surface coverage of GPDADMAC by phenol molecules leads to a linear decrease in the sorption energies. Moreover, the positive value of the constant, b, points to the fact that the adsorption process is exothermic. A comparative study of the performance of GPDADMAC with other materials from literature is presented in Table 4.

Table 3
Parameters of isotherm models for the adsorption of phenol by GPDADMAC

Langmuir	Freundlich	Temkin
R^2 = 0.992	R^2 = 0.948	R^2 = 0.9995
K_L (L g^{-1}) = 0.50	K_F (mg g^{-1}) = 1.38	K_T (mg g^{-1}) = 1.53
q_m (mg g^{-1}) = 4.54	n = 1.81	b (J mol^{-1}) = 2,400.5
R_L = 0.21		

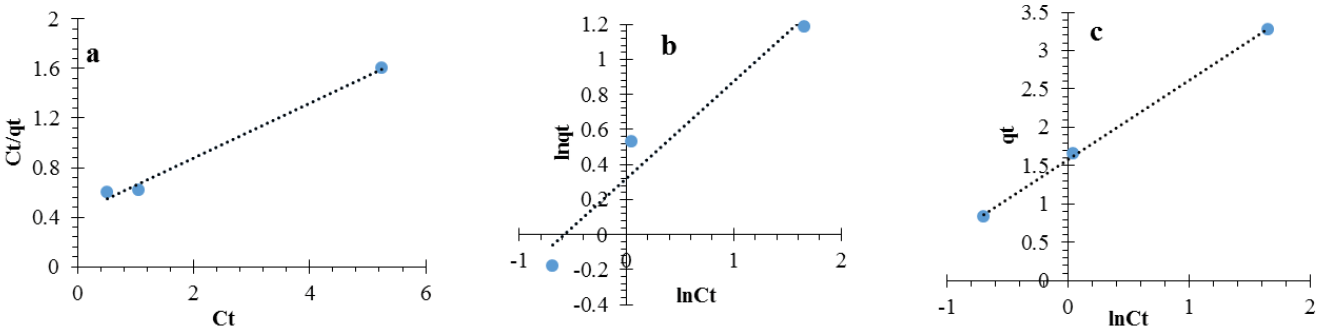

Fig. 8. (a) Langmuir isotherm plot, (b) Freundlich isotherm plot and (c) Temkin isotherm plot for phenol removal by GPDADMAC.

Table 4
Comparison of phenol adsorption performance of GPDADMAC with other materials from literature

Material	Adsorption capacity from (mg g^{-1})	% Phenol removal	Contact time	Initial phenol concentration	Adsorbent dosage	References
Activated carbon (AC)	1.348 (from Langmuir isotherm)	75%	2 h	2 mg L^{-1}	50 mg	[24]
Carbon nanotubes (CNTs)	1.098 (from Langmuir isotherm)	62%	2 h	2 mg L^{-1}	50 mg	[24]
Fly ash (FA)	1.007 (Langmuir isotherm)	60%	2 h	2 mg L^{-1}	50 mg	[24]
Carbon nanofibers (CNFs)	0.842 (Langmuir isotherm)	41%	2 h	2 mg L^{-1}	50 mg	[24]
Activated carbon from sawdust	0.022 (Langmuir isotherm)	–	3 h	20 mg L^{-1}	10 g L^{-1}	[56]
Graphene	18.6 (Experimental)	63.1%	48 h	50 mg L^{-1}	1.7 g L^{-1}	[57]
GPDADMAC	4.5413 (Langmuir isotherm	~80%	10 min	10 mg L^{-1}	400 mg	This work

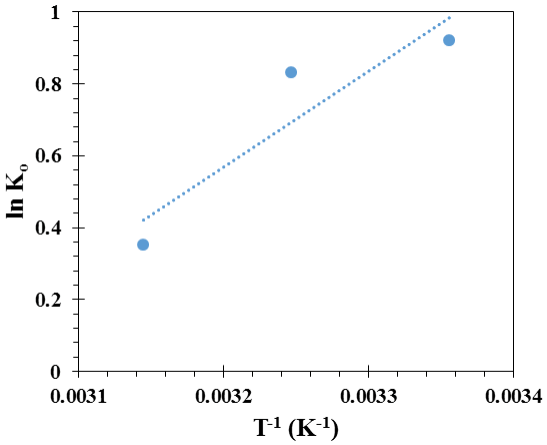

Fig. 9. Plot of ln K_0 vs. T^{-1}.

Table 5
Thermodynamics parameters for the adsorption of phenol by GPDADMAC

G (kJ mol^{-1})			H (kJ mol^{-1})	S (J mol^{-1} K^{-1})
298 K	308 K	318 K		
–0.21	–0.47	–2.77	–37.59	125.78

3.5. Thermodynamics

The thermodynamic model was investigated at absolute temperatures of 298, 308 and 318 K under the experimental conditions of 10 ppm initial phenol concentration, 4 g L^{-1} adsorbent dosage, 30 min contact time, 150 rpm agitation speed and initial solution pH of 6. From the plot of ln K_0 vs. T^{-1} displayed in Fig. 9, the enthalpy change (ΔH) and entropy change (ΔS) were, respectively, obtained from the slope and intercept. The negative value of ΔH suggests that the adsorption process was exothermic. Also, negative values of the ΔG at the different temperatures indicate the spontaneity of the adsorption process. There was increased randomness at the interface of the solution containing phenol and the GPDADMAC surface as suggested by the positive value of the ΔS. The values of (ΔH), (ΔS) and (ΔG) are summarized in Table 5.

4. Conclusion

A graphene-polymer adsorbent, GPDADMAC, was successfully synthesized by functionalizing graphene oxide with PDADMAC as evidenced by FTIR result. The potential of GPDADMAC to remove phenol from a single solute solution was investigated. The results of the batch adsorption experiments showed that the adsorbent removed about 80% of the phenol in solution within the first 10 min. The amount of phenol removed by GPDADMAC was quite stable under the influence of different initial solution pH, which implies that the adsorbent can perform within a wide range of pH. Kinetic modeling of the experimental data revealed that the pseudo-second-order model gave the best fit and therefore best explained the adsorption mechanics between phenol and GPDADMAC. Adsorption isotherm of experimental data were well represented by both Langmuir and Temkin models. In conclusion, the GPDADMAC can be considered a good adsorbent for phenol compared with other synthetic adsorbents.

Acknowledgments

The authors acknowledge the support of King Fahd University of Petroleum & Minerals (KFUPM) for the provision of finance and materials necessary for the completion of the research. T.A. Saleh would like to acknowledge the support and fund provided by King Fahd University of Petroleum & Minerals (KFUPM) through Project No. IN131053 under the Deanship of Research.

References

[1] M. Anbia, A. Ghaffari, Adsorption of phenolic compounds from aqueous solutions using carbon nanoporous adsorbent coated with polymer, Appl. Surf. Sci., 255 (2009) 9487–9492.
[2] J.C.G. Sousa, A.R. Ribeiro, M.O. Barbosa, M.F.R. Pereira, A.M.T. Silva, A review on environmental monitoring of water organic pollutants identified by EU guidelines, J. Hazard. Mater., 344 (2018) 146–162.
[3] A. Shet, S.K. Vidya, Solar light mediated photocatalytic degradation of phenol using Ag core – TiO_2 shell (Ag@TiO_2) nanoparticles in batch and fluidized bed reactor, Sol. Energy, 127 (2016) 67–78.
[4] H. Biglari, M. Afsharnia, V. Alipour, R. Khosravi, K. Sharafi, A.H. Mahvi, A review and investigation of the effect of nanophotocatalytic ozonation process for phenolic compound removal from real effluent of pulp and paper industry, Environ. Sci. Pollut. Res., 24 (2017) 4105–4116.
[5] J. Liu, J. Xie, Z. Ren, W. Zhang, Solvent extraction of phenol with cumene from wastewater, Desal. Wat. Treat., 51 (2013) 3826–3831.
[6] C. Liu, K. Han, D.J. Lee, Q. Wang, Simultaneous biological removal of phenol, sulfide, and nitrate using expanded granular sludge bed reactor, Appl. Microbiol. Biotechnol, 100 (2016) 4211–4217.
[7] Y. Cui, X.-Y. Liu, T.-S. Chung, M. Weber, C. Staudt, C. Maletzko, Removal of organic micro-pollutants (phenol, aniline and nitrobenzene) via forward osmosis (FO) process: evaluation of FO as an alternative method to reverse osmosis (RO), Water Res., 91 (2016) 104–114.
[8] E. Mousset, L. Frunzo, G. Esposito, E.D. van Hullebusch, N. Oturan, M.A. Oturan, A complete phenol oxidation pathway obtained during electro-Fenton treatment and validated by a kinetic model study, Appl. Catal., B, 180 (2016) 189–198.
[9] M.D. Víctor-Ortega, J.M. Ochando-Pulido, A. Martínez-Ferez, Performance and modeling of continuous ion exchange processes for phenols recovery from olive mill wastewater, Process Saf. Environ. Prot., 100 (2016) 242–251.
[10] S. De Gisi, G. Lofrano, M. Grassi, M. Notarnicola, Characteristics and adsorption capacities of low-cost sorbents for wastewater treatment: a review, Sustainable Mater.Technol., 9 (2016) 10–40.
[11] A.B. Albadarin, M.N. Collins, Mu. Naushad, S. Shirazian, G. Walker, C. Mangwandi, Activated lignin-chitosan extruded blends for efficient adsorption of methylene blue, Chem. Eng. J., 307 (2017) 264–272.
[12] Z.A. AL-Othman, R. Ali, Mu. Naushad, Hexavalent chromium removal from aqueous medium by activated carbon prepared from peanut shell: adsorption kinetics, equilibrium and thermodynamic studies, Chem. Eng. J., 184 (2012) 238–247.
[13] Mu. Naushad, T. Ahamad, Z.A. AlOthman, A.H. Al-Muhtaseb, Green and eco-friendly nanocomposite for the removal of toxic Hg(II) metal ion from aqueous environment: adsorption kinetics & isotherm modelling, J. Mol. Liq., 279 (2019) 1–8.

[14] A.A. Alqadami, Mu. Naushad, M.A. Abdalla, T. Ahamad, Z.A. ALOthman, S.M. Alshehri, A.A. Ghfar, Efficient removal of toxic metal ions from wastewater using a recyclable nanocomposite: a study of adsorption parameters and interaction mechanism, J. Cleaner Prod., 156 (2017) 426–436.
[15] M. Naushad, Surfactant assisted nano-composite cation exchanger: development, characterization and applications for the removal of toxic Pb^{2+} from aqueous medium, Chem. Eng. J., 235 (2014) 100–108.
[16] Mu. Naushad, T. Ahamad, G. Sharma, A.H. Al-Muhtaseb, A.B. Albadarin, M.M. Alam, Z.A. ALOthman, S.M. Alshehri, A.A. Ghfar, Synthesis and characterization of a new starch/SnO_2 nanocomposite for efficient adsorption of toxic Hg^{2+} metal ion, Chem. Eng. J., 300 (2016) 306–316.
[17] J. Wang, B. Chen, Adsorption and coadsorption of organic pollutants and a heavy metal by graphene oxide and reduced graphene materials, Chem. Eng. J., 281 (2015) 379–388.
[18] X. Wang, B. Liu, Q. Lu, Q. Qu, Graphene-based materials: fabrication and application for adsorption in analytical chemistry, J. Chromatogr. A, 1362 (2014) 1–15.
[19] W. Peng, H. Li, Y. Liu, S. Song, A review on heavy metal ions adsorption from water by graphene oxide and its composites, J. Mol. Liq., 230 (2017) 496–504.
[20] S. Wu, K. Zhang, X. Wang, Y. Jia, B. Sun, T. Luo, F. Meng, Z. Jin, D. Lin, W. Shen, L. Kong, J. Liu, Enhanced adsorption of cadmium ions by 3D sulfonated reduced graphene oxide, Chem. Eng. J., 262 (2015) 1292–1302.
[21] C. Liu, D. Zhang, L. Zhao, X. Lu, P. Zhang, S. He, G. Hu, X. Tang, Synthesis of a thiacalix[4]arenetetrasulfonate-functionalized reduced graphene oxide adsorbent for the removal of lead(II) and cadmium(II) from aqueous solutions, RSC Adv., 114 (2016) 113352–113365.
[22] V.K. Gupta, R. Kumar, A. Nayak, T.A. Saleh, M.A. Barakat, Adsorptive removal of dyes from aqueous solution onto carbon nanotubes: a review, Adv. Colloid Interface Sci., 193 (2013) 24–34.
[23] T.A. Saleh, A. Sarı, M. Tuzen, Effective adsorption of antimony(III) from aqueous solutions by polyamide-graphene composite as a novel adsorbent, Chem. Eng. J., 307 (2017) 230–238.
[24] L. Ji, W. Chen, Z. Xu, S. Zheng, D. Zhu, Graphene nanosheets and graphite oxide as promising adsorbents for removal of organic contaminants from aqueous solution, J. Environ. Qual., 42 (2013) 191–198.
[25] S. Chowdhury, R. Balasubramanian, Recent advances in the use of graphene-family nanoadsorbents for removal of toxic pollutants from wastewater, Adv. Colloid Interface Sci., 204 (2014) 35–56.
[26] B. Bolto, J. Gregory, Organic polyelectrolytes in water treatment, Water Res., 41 (2007) 2301–2324.
[27] R.K. Upadhyay, N. Soin, S.S. Roy, Role of graphene/metal oxide composites as photocatalysts, adsorbents and disinfectants in water treatment: a review, RSC Adv., 4 (2014) 3823–3851.
[28] B. Roig, C. Gonzalez, O. Thomas, Monitoring of phenol photodegradation by ultraviolet spectroscopy, Spectrochim. Acta, Part A, 59 (2003) 303–307.
[29] M. Thirumavalavan, Y.-L. Lai, L.-C. Lin, J.-F. Lee, Cellulose-based native and surface modified fruit peels for the adsorption of heavy metal ions from aqueous solution: langmuir adsorption isotherms, J. Chem. Eng. Data, 55 (2009) 1186–1192.
[30] F.A. Olabemiwo, B.S. Tawabini, F. Patel, T.A. Oyehan, M. Khaled, T. Laoui, Cadmium removal from contaminated water using polyelectrolyte-coated industrial waste fly ash, Bioinorg. Chem. Appl., 2017 (2017), doi.org/10.1155/2017/7298351.
[31] A. Nimibofa, E.N. Augustus, W. Donbebe, Modelling and interpretation of adsorption isotherms, J. Chem., 2017 (2017), doi.org/10.1155/2017/3039817.
[32] R.K. Gautam, A. Mudhoo, G. Lofrano, M.C. Chattopadhyaya, Biomass-derived biosorbents for metal ions sequestration: adsorbent modification and activation methods and adsorbent regeneration, J. Environ. Chem. Eng., 2 (2014) 239–259.
[33] A.A. Inyinbor, F.A. Adekola, G.A. Olatunji, Kinetics, isotherms and thermodynamic modeling of liquid phase adsorption of Rhodamine B dye onto *Raphia hookerie* fruit epicarp, Water Resour. Ind., 15 (2016) 14–27.
[34] Y. Zhang, D. Shao, J. Yan, X. Jia, Y. Li, P. Yu, T. Zhang, The pore size distribution and its relationship with shale gas capacity in organic-rich mudstone of Wufeng-Longmaxi Formations, Sichuan Basin, China, J. Nat. Gas Geosci., 1 (2016) 213–220.
[35] Y. Li, Q. Du, T. Liu, X. Peng, J. Wang, J. Sun, Y. Wang, S. Wu, Z. Wang, Y. Xia, L. Xia, Comparative study of methylene blue dye adsorption onto activated carbon, graphene oxide, and carbon nanotubes, Chem. Eng. Res. Des., 91 (2013) 361–368.
[36] K. Soleimani, A.D. Tehrani, M. Adeli, Bioconjugated graphene oxide hydrogel as an effective adsorbent for cationic dyes removal, Ecotoxicol. Environ. Saf., 147 (2018) 34–42.
[37] M. Şinoforoğlu, B. Gür, M. Arık, Y. Onganer, K. Meral, Graphene oxide sheets as a template for dye assembly: graphene oxide sheets induce H-aggregates of pyronin (Y) dye, RSC Adv., 3 (2013) 11832–11838.
[38] D.-Q. Yang, J.-F. Rochette, E. Sacher, Spectroscopic evidence for π−π interaction between poly(diallyl dimethylammonium) chloride and multiwalled carbon nanotubes, J. Phys. Chem. B, 109 (2005) 4481–4484.
[39] V. Ţucureanu, A. Matei, A.M. Avram, FTIR spectroscopy for carbon family study, Crit. Rev. Anal. Chem., 46 (2016) 502–520.
[40] L. Ding, Y. Liu, S.-X. Guo, J. Zhai, A.M. Bond, J. Zhang. Phosphomolybdate@poly(diallyldimethylammonium chloride)-reduced graphene oxide modified electrode for highly efficient electrocatalytic reduction of bromate, J. Electroanal. Chem., 727 (2014) 69–77.
[41] H. Li, L.-P. Jia, R.-N. Ma, W.-L. Jia, H.-S. Wang, Electrodeposition of PtNPs on the LBL assembled multilayer films of (PDDA-GS/PEDOT:PSS)$_n$ and their electrocatalytic activity toward methanol oxidation, RSC Adv., 7 (2017) 16371–16378.
[42] H. Li, K. Sheng, Z. Xie, L. Zou, B. Ye, Highly sensitive determination of hyperin on poly(diallyldimethylammonium chloride)-functionalized graphene modified electrode, J. Electroanal. Chem., 776 (2016) 105–113.
[43] M. Huang, X. Xu, H. Yang, S. Liu, Electrochemically-driven and dynamic enhancement of drug metabolism *via* cytochrome P450 microsomes on colloidal gold/graphene nanocomposites, RSC Adv., 2 (2012) 12844–12850.
[44] J. Coates, Interpretation of infrared spectra, a practical approach, Encycl. Anal. Chem. Appl. Theory Instrum., 12 (2000) 10815–10837.
[45] S. Yu, X. Wang, W. Yao, J. Wang, Y. Ji, Y. Ai, A. Alsaedi, T. Hayat, X. Wang, Macroscopic, spectroscopic, and theoretical investigation for the interaction of phenol and naphthol on reduced graphene oxide, Environ. Sci. Technol., 51 (2017) 3278–3286.
[46] H. Ren, D.D. Kulkarni, R. Kodiyath, W. Xu, I. Choi, V.V. Tsukruk, Competitive adsorption of dopamine and rhodamine 6G on the surface of graphene oxide, ACS Appl. Mater. Interfaces, 6 (2014) 2459–2470.
[47] M.T. McDermott, R.L. McCreery, Scanning tunneling microscopy of ordered graphite and glassy carbon surfaces: electronic control of quinone adsorption, Langmuir, 10 (1994) 4307–4314.
[48] X. Wang, S. Huang, L. Zhu, X. Tian, S. Li, H. Tang, Correlation between the adsorption ability and reduction degree of graphene oxide and tuning of adsorption of phenolic compounds, Carbon, 69 (2014) 101–112.
[49] W. Chen, L. Duan, L. Wang, D. Zhu, Adsorption of hydroxyl- and amino-substituted aromatics to carbon nanotubes, Environ. Sci. Technol., 42 (2008) 6862–6868.
[50] Y.E. Dolaksiz, F. Temel, M. Tabakci, Adsorption of phenolic compounds onto calix[4]arene-bonded silica gels from aqueous solutions, React. Funct. Polym., 126 (2018) 27–35.
[51] O. Abdelwahab, N.K. Amin, Adsorption of phenol from aqueous solutions by *Luffa cylindrica* fibers: kinetics, isotherm and thermodynamic studies, Egypt. J. Aquat. Res., 39 (2013) 215–223.
[52] K. Smets, M. De Jong, I. Lupul, G. Gryglewicz, S. Schreurs, R. Carleer, J. Yperman, Rapeseed and raspberry seed cakes as inexpensive raw materials in the production of activated carbon

by physical activation: effect of activation conditions on textural and phenol adsorption characteristics, Materials, 9 (2016) 565.
[53] P.-R. Liu, H.-L. Zhang, T. Wang, W.-L. Yang, Y. Hong, Y.-L. Hou, Functional graphene-based magnetic nanocomposites as magnetic flocculant for efficient harvesting of oleaginous microalgae, Algal Res., 19 (2016) 86–95.
[54] H.A. Asmaly, B. Abussaud, Ihsanullah, T.A. Saleh, A.A. Bukhari, T. Laoui, A.M. Shemsi, V.K. Gupta, M.A. Atieh, Evaluation of micro- and nano-carbon-based adsorbents for the removal of phenol from aqueous solutions, Toxicol. Environ. Chem., 97 (2015) 1164–1179.
[55] H.A. Asmaly, Ihsanullah, T.A. Saleh, T. Laoui, V.K. Gupta, M.A. Atieh, Enhanced adsorption of phenols from liquids by aluminum oxide/carbon nanotubes: comprehensive study from synthesis to surface properties, J. Mol. Liq., 206 (2015) 176–182.
[56] S. Larous, A.-H. Meniai, The use of sawdust as by product adsorbent of organic pollutant from wastewater: adsorption of phenol, Energy Procedia, 18 (2012) 905–914.
[57] Y. Li, Q. Du, T. Liu, J. Sun, Y. Jiao, Y. Xia, L. Xia, Z. Wang, W. Zhang, K. Wang, H. Zhu, D. Wu, Equilibrium, kinetic and thermodynamic studies on the adsorption of phenol onto graphene, Mater. Res. Bull., 47 (2012) 1898–1904.